PREDICTING ELECTROCHEMICAL BREAKDOWN IN TERRESTRIAL PHOTOVOLTAIC MODULES*

by

Gordon R. Mon+,
John Orehotsky++,
Ronald G. Ross, Jr.+++,
Guy Whitla+

Jet Propulsion Laboratory
California Institute of Technology
Pasadena, California

ABSTRACT

Results of recent investigations of electrochemical corrosion in terrestrial photovoltaic modules are presented. Tests on encapsulated two-cell coupons have yielded electrical and visual information that reveals the nature of the degradation mechanism and quantitative dependencies among measured variables. Data are interpreted to imply that a fixed level of charge transfer at the metallization-encapsulation interface results in a fixed percentage of cell failures. The method developed to determine median time to cell failure uses measured encapsulant conductivities and site-specific weather data. A log-normal distribution of failure times is assumed, enabling determination of general cell and module failure rates.

INTRODUCTION

The Engineering Sciences Area of the Jet Propulsion Laboratory's Flat-Plate Solar Array Project has the responsibility within the Department of Energy's National Photovoltaics Program for performing research aimed at improving photovoltaic module reliability. To achieve this goal, researchers must identify and determine the causes and the physical processes - i.e., the mechanism - underlying the degradation that compromises module reliability. With this understanding, design improvements can be incorporated that enhance module performance; also, with knowledge of failure rates at use conditions, service lifetime can be predicted, allowing more accurate system cost projections to be made.

The particular module degradation mechanism addressed in this paper is electrochemical corrosion. A schematic, qualitative representation of the mechanism is depicted in Figure 1. A voltage difference between two electrified cells, or between an electrified cell and grounded frame, may result in dissolution of cell metallization material into the surrounding encapsulant. Driven by voltage and concentration gradients, the dissolved metallization ions diffuse through the encapsulant (wavy arrows, Figure 1) to the cathode whereon they deposit to form metallic dendrites. These "grow" back toward the anode until the intervening encapsulation becomes insufficiently resistive to prevent the formation of a gap-bridging channel and the consequent electrical breakdown of the insulation.

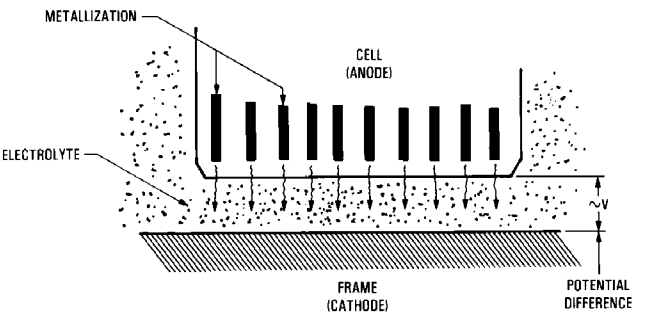

Figure 1. The Electrochemical Corrosion Mechanism

Electrochemical solar-cell corrosion was first observed in accelerated long-term bias-temperature-humidity tests conducted on behalf of the Flat-Plate Solar Array Project by Wyle Laboratories. The phenomenon was observed on cells with both Ti-Pd-Ag (passivated silver, tri-metal) and printed silver metallization systems (Figure 2). These cells

---

*This paper presents the results of one phase of research conducted at the Jet Propulsion Laboratory, California Institute of Technology, and sponsored by the U.S. Department of Energy through an agreement with the National Aeronautics and Space Administration.

+Member of the Technical Staff, Flat-Plate Solar Array Project, Energy Technology Engineering Section, Jet Propulsion Laboratory, California Institute of Technology, Pasadena, California, 91109.

++Professor of Engineering, Wilkes College, Wilkes-Barre, Pennsylvania, 18766.

+++Engineering Sciences Manager, Flat-Plate Solar Array Project, and Supervisor, Photovoltaic Engineering Section, Jet Propulsion Laboratory, California Institute of Technology, Pasadena, California, 91109.

Figure 2. Solar-Cell Electrochemical Corrosion

resided in modules that were forward biased at 100 mA while exposed to an 85°C/85% RH environment for 180 days. Various terms such as gridline blossoming, spreading, and Q-tipping were originally used to describe the observed phenomenon that is now referred to as electrochemical corrosion. Electrochemical corrosion has since been observed at field-test sites (JPL), at applications sites (Southwest Residence, Las Cruces, New Mexico) and in extensive laboratory tests conducted by several investigators at JPL. These tests, undertaken to reveal and quantify the physical process of electrochemical corrosion, have yielded a significant body of data, a portion of which is analyzed and interpreted here.

PRELIMINARIES

The problem of electrochemical degradation of metallized silicon, although only recently observed in solar cells, is not new to the silicon semiconductor device industry. Ghate (1) discusses electromigration-induced failures in VLSI thin-film interconnects and gives several historical references dating back to 1967. In two papers Sbar (2,3) and coworkers reported their investigations of electrochemical and galvanic corrosion of copper-based metallizations at 85°C/80% RH in corrosive (Cl_2, SO_2) environments. In another paper Sbar and Kozakiewicz (4) developed surface conductance acceleration factors that relate device life in high temperature/humidity laboratory environments to device life in normal use environments; they used these acceleration factors to predict electrolytic corrosion failure rates on active devices from measured failure rates at accelerated stress conditions. The research discussed in this present paper is similar in nature and supports many of the findings and conclusions of Sbar's work, which is cited often in this text.

EXPERIMENTAL INVESTIGATIONS

Unencapsulated Solar-Cell Experiments

After the initial observation of solar-cell metallization migration in the long-term Wyle test modules, experiments were undertaken to identify a suitable index of electrochemical degradation and to determine associated degradation rates. In one experiment, unencapsulated solar-cell electrodes were immersed in a 0.0001 molar aqueous electrolyte while current levels of 0.01 amperes to 0.0001 amperes were maintained between them. The cells were periodically removed from the electrolyte and their maximum power outputs were measured using an I-V curve tracer. These data are presented in Figure 3 as a plot of time to 25% power reduction versus current density.

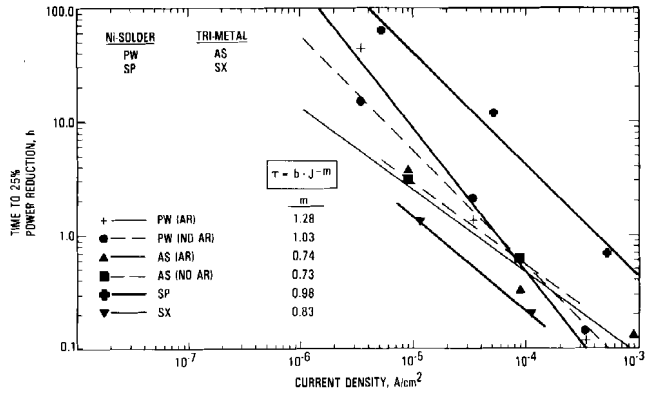

Figure 3. Time to 25% Maximum Power Degradation versus Current Density ($H^+ = 10^{-4}$ Molar)

Figure 3 shows that the Ni-solder metallizations require a greater charge transfer for a particular time to failure--at least under conditions of aqueous immersion--than do passivated silver metallizations. Also, the presence or absence of anti-reflective cell coatings (AR, Figure 3) has little effect on the experimental outcome. Because much is unknown about the proprietary metallization formulations, these observations are made without interpretation. It is clear, however, that for a particular metallization system, it is possible to associate a particular quantity of charge transfer with a particular time to failure, an observation that is exploited below to predict the service life of photovoltaic modules.

Encapsulated Solar-Cell Experiment

Since unencapsulated solar cells immersed in an aqueous electrolyte degrade rapidly, they provide a convenient means of observing electrochemical

degradation and studying comparative performance of metallizations in the laboratory. But deployed cells are almost always encapsulated and generally not deliberately immersed in aqueous solution. Encapsulated two-cell coupons (Figure 4) were specially fabricated to study the response of photovoltaic constructions to induced electrochemical corrosion under controlled laboratory conditions. These conditions--85°C/2.5% RH, 85°C/70% RH, and 85°C/98% RH--were maintained to within 2% nominal by Blue-M environmental chambers.

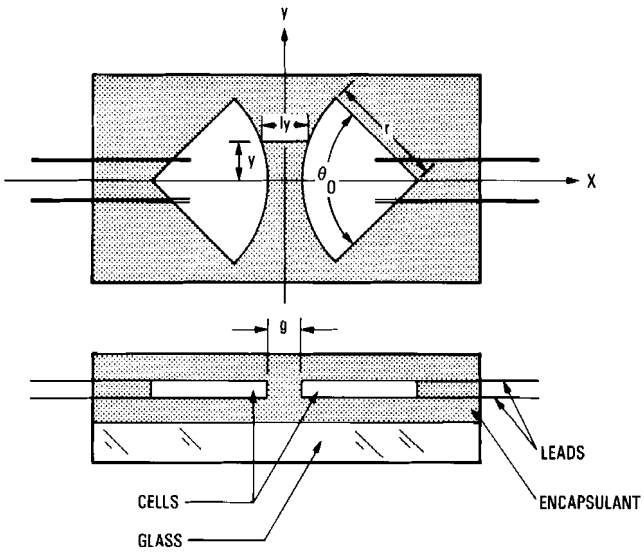

Figure 4. Electrochemical Corrosion Test Specimen Geometry

The 85°C temperature was selected because it is an often-used accelerated test temperature (2-5); at this temperature the 10°C-Rule approximation to the Arrhenius temperature acceleration model, which states that for each 10°C increment in temperature the rate (of electrochemical reaction) doubles (6), yields an acceleration factor of 15 (7) over the 46°C daytime cell temperature expected in a typical field deployment (8).

Sample geometry is depicted in Figure 4; samples consisted of two commercial solar cells encapsulated in two layers (≃0.1 cm total) of commercial pottant, all mounted on a 0.32-cm-thick glass support. Three different encapsulants: polyvinyl butyral (PVB), silicone rubber (RTV), and ethylene vinyl acetate (EVA), and three different cell metallizations: silver paste, tri-metal, and Ni-solder, were tested; in combination, these gave nine different sample types.

Three samples of each type were exposed in each chamber for a total of 1944 hours; of the three, one was electrified at 60 volts cell-to-cell, one at 30 volts cell-to-cell, and one--the control, to enable differentiation of electro-chemical from galvanic and non-electrical effects--remained unelectrified.

Measurements were electrical and visual. Electrical measurements included pre- and post-exposure I-V characteristics of each cell. All other electrical measurements were made in situ before and after exposure (ambient conditions) and five times during exposure (test conditions). These included (1) cell measurements: junction capacitance and loss factor; and (2) insulation measurements: insulation capacitance, insulation loss factor, insulation resistance and discharge inception voltage. These variables were monitored to determine if one or more of them could serve as an easily obtainable measure of module electrochemical corrosion. Some are traditional measures of aging, some are not.

Visual measurements took the form of a post-test inspection under low-power (50X) optical magnification, after which specimens were prepared for microexamination (SEM, EDAX, ESCA, Auger surface analysis, etc.).

Although the analysis and interpretation of this sizeable data base will be useful in module design, only those data directly relevant to module life prediction are further considered here.

DATA

Visual and Power Observations

After 1944 hours of exposure, the RTV- and EVA-encapsulated samples exhibited no obvious degradation other than apparent cell surface stains in the high-humidity (85°C/98% RH) environment. The PVB-encapsulated samples, on the other hand, exhibited pronounced discoloration of the encapsulation, and electromigration, both of which worsened with humidity and applied voltage.

From pre- and post-exposure I-V curves, it was generally found that the maximum power output decreased as a result of a combination of factors: reduction of short-circuit current, increase of series resistance, and decrease of shunt resistance. The reduction of short-circuit current was attributed to optical transmission losses in the discolored encapsulant above the solar cell. Increase of series resistance was generally associated with electrochemical corrosion and/or debonding of the cell metallization. Decrease of shunt resistance was attributed to external current paths that circumvent the solar-cell junction. In particular, changes in shunt resistance contribute significantly to power reductions in silver-print and tri-metal cells, and short-circuit current losses were found to contribute significantly to power reductions in PVB- encapsulated samples. This is consistent with the observed excessive electromigration in silver-metallized cells and the severe discoloration of the PVB encapsulation.

Data Analysis

For anode cells in the PVB- and EVA-encapsulated samples, the ratio of post- to pre-exposure cell power output was plotted (Figure 5) against total

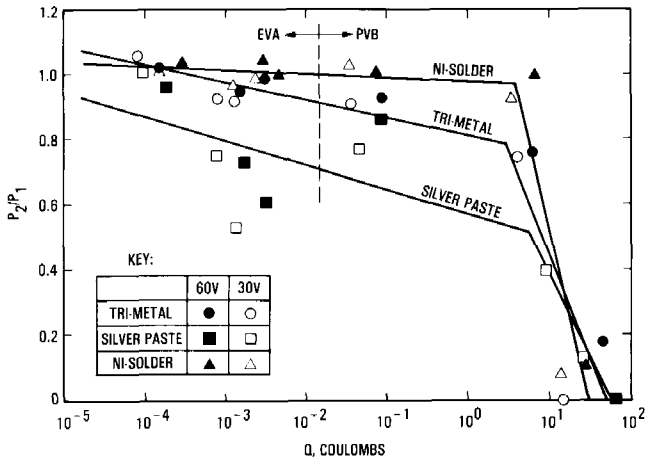

Figure 5. Normalized Cell Output versus Interfacial Charge Transferred in 1944 Hours of Test Exposure

charge transferred from anode to cathode. The plot suggests two groupings of data--one nearly horizontal, the other nearly vertical. It appears that power reduction is gradual until about Q_T = 4 coulombs of charge per 10 cm of edge length have been transferred, regardless of metallization, after which the cell power output drops rapidly. This is consistent with the view that failure occurs only after a quantity of cell metallization has dissolved into the encapsulant, has migrated to the cathode, and has formed a short-circuit path between anode and cathode.

The uncertainty in the data, or their repeatability, have not been determined.

The charge transferred was calculated from Ohm's law:

$$I = V \cdot Y = V \cdot \kappa \int_0^{\theta_0} \frac{t}{l_y}\, dy \qquad (1)$$

valid for round cells, and

$$Q = I \cdot \tau \qquad (2)$$

where

Q = charge transferred, coulombs
I = current, amperes
τ = test time, 1944 hours
V = test application voltage, volts
Y = cell-to-cell conductance, Ω^{-1}
κ = insulation electrical conductivity, Ω^{-1} cm^{-1}
t = effective electromigration thickness, cm
l_y = cell-to-cell distance (see Figure 4) at point y, cm.

Combining Equations 1 and 2 and performing the integration leads to

$$Q = V \cdot (\kappa\tau) \cdot t\, II \qquad (3)$$

where

$$II = \int_0^{\theta_0} \frac{dy}{l_y} = \frac{2}{K+1}\left[\frac{K}{L} \cdot \tan^{-1}\left(\frac{1}{L}\tan\frac{\theta_0}{4}\right) - (K+1)\frac{\theta_0}{4}\right] \qquad (4)$$

$$L = \sqrt{\frac{K-1}{K+1}} \qquad (5)$$

$$K = 1 + \frac{g}{2r} \qquad (6)$$

See Figure 4 for definitions of the variables g, r, and θ_0.

Several assumptions, approximations, and experimental measurements, discussed below, contribute to the charge transfer values determined by using Equation 3; in particular, the variables κ and t require elaboration.

The finding of the coatings industry (9-12) that high coating conductance correlates strongly with substrate corrosion (and vice versa) is manifested in Equation 3 as a linear dependence between charge transferred and insulation conductivity. The actual conductivity values used were experimentally obtained by measuring the current between electrified parallel plane electrodes embedded in slabs of PVB and EVA. Preliminary data were gathered at several temperature and humidity combinations. A functional relationship of the form

$$\log\frac{1}{\kappa} = a_0 + a_1 h + a_2 h^2 + b_1\beta + b_2\beta^2 + c_1 h\beta \qquad (7)$$

was fitted to the global data set for each material using a nonlinear least-squares minimization routine based upon the variable metric method of Davidon (13) as modified by Fletcher and Powell (14). The expression for PVB is

$$\log\frac{1}{\kappa} = 9.91 - 3.39h + 0.694h^2 + 2.63\beta + 0.639\beta^2 + 0.16h\beta \qquad (8)$$

and for EVA,

$$\log\frac{1}{\kappa} = 12.41 - 2.06\,h + 0.977h^2 + 2.38\beta + 0.00513\beta^2 - 0.0572h\beta \qquad (9)$$

These expressions are plotted in Figure 6. In Equations 7 through 9,

$$h = \frac{RH}{100},\ 0 \le h \le 1 \qquad (10)$$

and

$$\beta = \frac{1519.76}{T + 273} - 4.19, \quad 0^{\circ}C \leq T \leq 100^{\circ}C \qquad (11)$$

where RH is the relative humidity, %, and T is the temperature, °C.

In using Equation 3 to compute the charge values of Figure 5, it was assumed that the κ values determined from Figure 6 for the three T/RH combinations of the experiment did not change during the 1944-hour duration of the test.

Finally, the effective electromigration thickness t appearing in the integral in Ohm's law, Equation 1, was taken to be three times the cell thickness, because electromigration from cell-to-cell was observed to have an out-of-plane component, contaminating the encapsulation about one cell's thickness above and below the top and bottom surfaces of the cell. The insulation thickness is about three times the cell thickness and may also serve as t in Equations 1 and 3. Computer mapping of the specimen field lines (15) also indicates the out-of-plane component impacting about one cell thickness above and below the cell surfaces.

LIFE PREDICTION

It is known that at the mechanism level a measure of electrochemical corrosion is the quantity of charge transferred at the metallization-encapsulation interface (16). This fact suggests that at the cell level, quantity of charge transferred between an edge cell and the module frame may be a reliable measure of the life of that cell-frame interface region. That being the case, module failure rates become calculable for model arrays.

To accomplish this, the test data from Figure 5 are first interpreted to imply that median time to cell failure occurs after a determinable quantity Q_T of charge has transferred from electrified cell to ground. This quantity of transferred charge, together with site-specific SOLMET weather data and encapsulant electrical conductivity values, determine the yearly daylight-hour charge transfer Q_Y. Then the median time to cell failure is $\tau_M = Q_T/Q_Y$. A log-normal distribution of cell failure times is assumed and a realistic standard deviation is borrowed from the work of Sbar (4), who experimentally determined electrochemical failure statistics of digital ICs. Thus, general failure rates of photovoltaic cells suffering electrochemical corrosion become determinable.

Statistical considerations applied to a model array field lead to expressions for module failure rates--in particular, the average yearly fraction of module failures. This quantity in turn determines expected replacement costs when calculating the life-cycle cost of delivered energy (17, 18).

Prediction of Cell Median Life

Consider now a single electrified cell adjacent to a grounded module frame. Figure 5 is interpreted to imply that, after the passage of $Q_T = 4$ coulombs of charge between cell and frame, the cell will have failed (electrochemical breakdown) with a probability of 0.50; the time necessary for the passage of this quantity of charge is the median time to failure. It is evaluated in this paper at three sites for which SOLMET weather data exist: Albuquerque, Boston, and Miami. Using hourly weather analysis, the SOLMET data are reduced to the form of daylight (insolation > 5 mW/cm^2) hours spent per year at various T/RH combinations (see Table 1). The temperature T is the cell temperature; RH is the computed relative humidity internal to the photovoltaic module, based upon the hourly cell temperature T and the hourly ambient air temperature-humidity status (7).

To every entry τ (T, RH) of this operating condition matrix, there corresponds a value κ (T, RH) obtainable from Figure 6 or from Equations 8 through 11; multiply these and sum the products to obtain $\Sigma\kappa_i\tau_i$ for each material (PVB and EVA) at each site (Table 2).

The prediction of median life is attempted for both a round and a rectangular cell adjacent to a module frame. The pertinent geometry for the round cell is shown in Figure 4, with the Y-axis taken as the grounded frame and the gap taken as g/2 (not g). For this case, the yearly charge transfer is (cf. Equation 3):

$$Q_Y = 2V\ (\Sigma\kappa_i\tau_i)\ t\ \text{II} \qquad (12)$$

For a rectangular cell at a distance g/2 from the module frame, Ohm's law yields

$$Q_Y = 2V\ (\Sigma\kappa_i\tau_i)\ t\ \frac{s}{g} \qquad (13)$$

where s is the length of the cell edge adjacent and parallel to the frame. Note that the quantity $\Sigma\kappa_i\tau_i$, tabulated in Table 2, appears in Equations 12 and 13.

The median time to failure, τ_M, is now given as

$$\tau_M = \frac{Q_T}{Q_Y} \qquad (14)$$

with $Q_T = 4$ coulombs per 10 cm of cell-frame edge.

Equations 12 through 14 exhibit the proportional dependence of median cell life on encapsulant resistivity determined experimentally by Sbar and Kozakiewicz (4).

The median time to cell failure was computed for the three chosen geographic sites for three different voltages, three different cell-to-frame distances, and two encapsulations; the dependency on these parameters of median time to failure is presented in Table 3.

It is observed that median cell lifetime increases as the cell-frame separation increases, more rapidly for rectangular than for round cells; that median life decreases proportionately with increasing voltage; and that round cells have

Table 1. SOLMET Weather Data: Hours per Year at T/RH Combinations Listed (Insolation > 5 mW/cm^2)

	Module Temp., C	Module RH, % 5	15	25	35	45	55	65	75	85	95
	85	0	0	0	0	0	0	0	0	0	0
	75	2	0	0	0	0	0	0	0	0	0
	65	303	0	0	0	0	0	0	0	0	0
	55	579	34	0	0	0	0	0	0	0	0
Albuquerque	45	537	182	4	0	0	0	0	0	0	0
	35	522	217	123	33	3	0	0	0	0	0
	25	196	264	92	77	44	39	10	3	1	0
	15	20	152	150	79	32	15	15	3	2	0
	5	0	16	47	51	48	32	16	10	2	0
	85	0	0	0	0	0	0	0	0	0	0
	75	0	0	0	0	0	0	0	0	0	0
	65	0	0	0	0	0	0	0	0	0	0
	55	97	101	0	0	0	0	0	0	0	0
Boston	45	131	273	91	4	0	0	0	0	0	0
	35	104	211	164	104	60	10	0	0	0	0
	25	81	201	140	118	104	106	75	28	10	0
	15	39	91	112	86	79	80	78	92	42	1
	5	3	22	39	68	72	78	60	48	35	0
	85	0	0	0	0	0	0	0		0	0
	75	0	0	0	0	0	0	0	0	0	0
	65	4	27	0	0	0	0	0	0	0	0
	55	66	663	124	0	0	0	0	0	0	0
Miami	45	35	296	546	282	8	0	0	0	0	0
	35	11	43	158	292	372	224	81	2	0	0
	25	0	11	25	58	82	131	151	151	23	0
	15	0	0	2	5	16	10	8	8	6	0
	5	0	0	0	0	1	1	0	0	0	0

longer median lifetimes than rectangular cells, other things being equal--because more of the periphery of rectangular cells is adjacent to the module frame. The superiority of EVA in extending cell median life by at least two orders of magnitude beyond that expected with PVB is noted.

Finally, as expected, median life is shorter in hot, humid Miami than in colder, drier Boston.

Cell Failure Rates

With the time for 50% cell failures established, the time for an arbitrary percentage of cell failures is now determined.

It is assumed that the natural logarithms of the cell failure times are normally distributed with mean μ and standard deviation σ. The density function is

$$f(\tau) = \frac{1}{\sqrt{2\pi}\sigma} \exp\left[-\frac{1}{2}\left(\frac{\ln \tau - \mu}{\sigma}\right)^2\right] \qquad (15)$$

The fraction of cells that fail in year t is

$$p(t) = \int_{\ln (t-1)}^{\ln t} f(\tau) d(\ln \tau) \qquad (16)$$

Under the change of variable

$$\eta = \frac{1}{\sigma} (\mu - \ln \tau) \qquad (17)$$

Equation 16 becomes

$$p(t) = \int_{\eta_t}^{\eta_{t-1}} \frac{1}{\sqrt{2\pi}} \exp -\left[\frac{1}{2}\eta^2\right] d\eta \qquad (18)$$

where

$$\eta_t = \frac{1}{\sigma} (\mu - \ln \tau) \qquad (19)$$

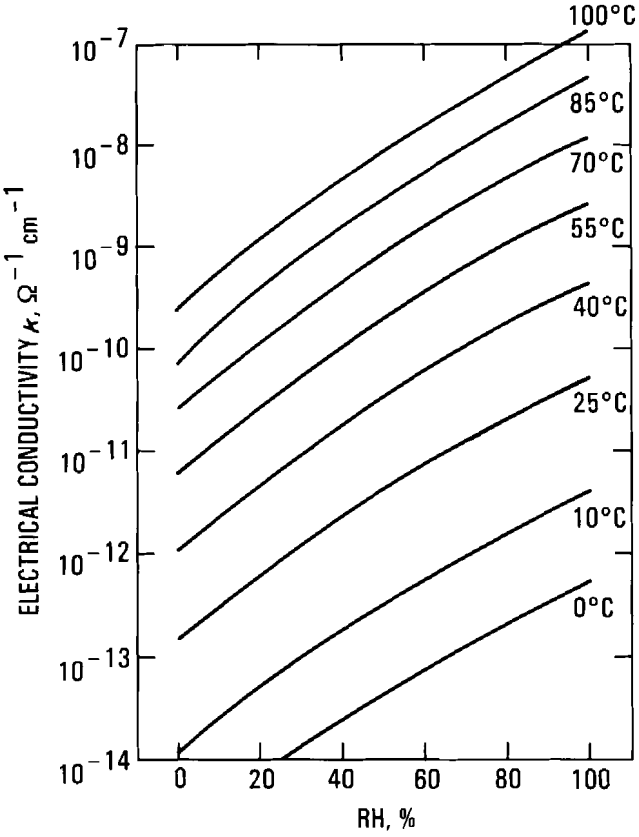

Figure 6a. Electrical Conductivity, PVB

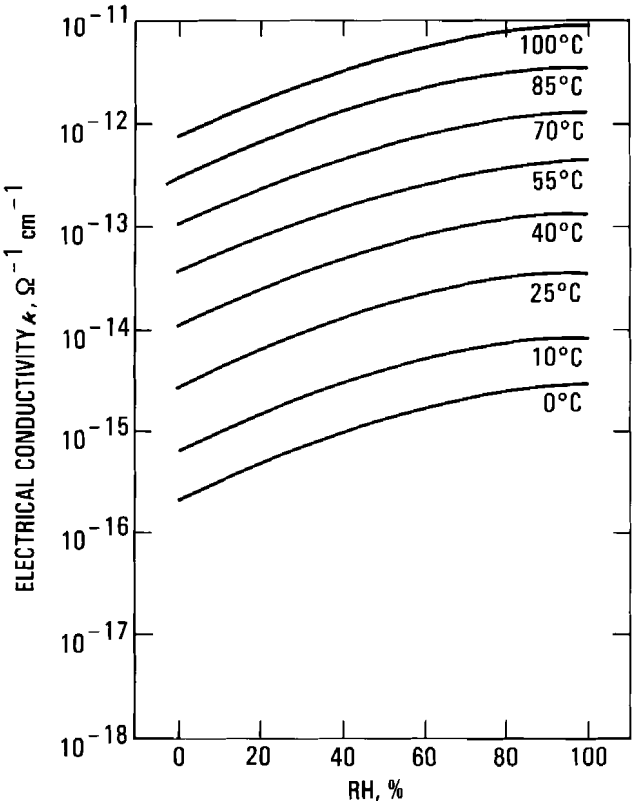

Figure 6b. Electrical Conductivity, EVA

Now for log-normal statistics, the median is (19):

$$\tau_M = \exp(\mu) \qquad (20)$$

where τ_M is the median time to failure.

Then, from Equations 19 and 20,

$$\eta_t = -\frac{1}{\sigma} \ln \frac{t}{\tau_M} \qquad (21)$$

To determine cell failure rates, first determine the median time to failure (Equation 14), specify the standard deviation σ, obtain η_t and η_{t-1} for the year t of interest (Equation 21), and finally obtain the probability p(t) (Equation 18) that a cell fails in the t^{th} year.

Module Failure Rates

It is assumed that only cells adjacent to a module frame are subject to failure by electrochemical corrosion. Then the probability that a module fails in year t, is the probability that at least one edge cell of that module fails in year t

Table 2. The Quantity $\Sigma\kappa_i\tau_i$ for PVB and EVA at Selected Sites

Site	$\Sigma\kappa_i\tau_i$ (Ω^{-1} cm^{-1} s/y)	
	PVB	EVA
Albuquerque	6.80×10^{-5}	3.16×10^{-7}
Boston	4.54×10^{-5}	1.84×10^{-7}
Miami	2.06×10^{-4}	5.98×10^{-7}

but none before year t; from probability theory, this is

$$Q_t = \left[1 - \sum_{i=1}^{t-1} Q_i\right] \cdot q(t), \quad t > 1 \qquad (22)$$

$$q(t) = 1 - \left[1 - p(t)\right]^{r+4} \qquad (23)$$

Table 3. Median Time to Failure, Exhibiting Dependency on Site, Encapsulation, Voltage, and Cell-to-Frame Distance

$r = 5$ cm, $\theta_0 = \pi$	$t = 0.114$ cm	Round Cells in PVB			Round Cells in EVA		
		τ_M, Years			τ_M, Years		
Cell-to-Frame Voltage, Volts	Cell-to-Frame Distance, cm	Albuquerque	Boston	Miami	Albuquerque	Boston	Miami
250	0.0635	59.6	89.3	19.7	12,800	22,000	6,800
	0.254	135.1	202.5	44.6	29,100	50,000	15,400
	0.635	245.7	368.2	81.1	52,900	91,000	27,900
500	0.0635	29.8	44.7	9.8	6,400	11,000	3,400
	0.254	67.6	101.2	22.3	14,600	25,000	7,700
	0.635	122.9	184.1	40.6	26,500	45,400	14,000
1000	0.0635	14.9	22.3	4.9	3,200	5,500	1,700
	0.254	33.8	50.6	11.2	7,300	12,500	3,800
	0.635	61.4	92.0	20.3	13,200	23,000	7,000
$s = 10$ cm	$t = 0.114$ cm	Rectangular Cells in PVB			Rectangular Cells in EVA		
		τ_M, Years			τ_M, Years		
Cell-to-Frame Voltage, V	Cell-to-Frame Distance, cm	Albuquerque	Boston	Miami	Albuquerque	Boston	Miami
250	0.0635	12.7	19.0	4.2	2,700	4,700	1,400
	0.254	50.6	75.8	16.7	10,900	18,700	5,800
	0.635	126.5	189.6	41.8	27,300	46,700	14,400
500	0.0635	6.3	9.5	2.1	1,400	2,300	720
	0.254	25.3	37.9	8.4	5,500	9,300	2,900
	0.635	63.3	94.8	20.9	13,600	23,300	7,200
1000	0.0635	3.2	4.7	1.0	700	1,167	360
	0.254	12.7	18.8	4.2	2,700	4,700	1,400
	0.635	31.6	47.4	10.4	6,800	11,700	3,600

where $Q_1 = q(1)$ and

$q(t)$ = probability that the module fails in year t given that it has not failed before year t

$p(t)$ = probability of electrochemical failure in year t of an adjacent cell-frame gap, Equation 18

r = the number of cells adjacent to the module periphery

In Equation 23 it is assumed that $p(t)$ is the same for all edge cells of a particular module. This is equivalent to assuming that module voltage is constant, a good assumption considering that inthe 1 x 4 ft and 4 x 4 ft modules currently used in central-station arrays, the voltage differential between module terminals is about 5 volts, whereas system operating voltages may range from 250 to 1000 volts or more. The module operating voltage is taken to be the mean of the module terminal voltages.

The exponent r + 4 in Equation 23 reflects the fact that corner cells are counted twice, as they are adjacent to two sections of the module frame.

Consider now an N-module series string in an array source circuit. The yearly average module failure probability is

$$\overline{Q}_t = \frac{1}{N} \sum_{K=1}^{N} Q_t^K \qquad (24)$$

where K denotes the K^{th} module in the N-module series string.

A computer code, incorporating the concepts and equations introduced here, was developed to compute the yearly fraction of modules that fail in a model array. A typical output from that program is presented in Figure 7, in which yearly average module failure probability is plotted against years of operation. Only one case is depicted--that of a 1000-volt array in Miami featuring EVA-encapsulated 4 x 4 ft modules having 10 cm square cells.

For comparison with these data, Ross (20), in a companion paper at this conference, develops target failure-rate allocations for the various possible cell and module failure mechanisms. He points out that the economic impact of module failures is greatest in the early years of array operation, since later-year replacement costs and energy revenue are more heavily discounted. Assuming a linearly increasing failure rate, he defines the allowable module failure level for electrochemical corrosion as 0.0001 failures per year per year. This provides a target level for comparison with the several examples computed here. The 10-year slope for the specific example of Figure 7 is compared with the maximum allowable slope of 0.0001 failures per year per year. If the module failure rate curve peaks before 10 years, as is the case with all of the PVB examples, then the calculated slope is that of the line of maximum slope from the origin to the failure-rate curve. The results of the calculations of failure-rate slopes are presented in Table 4. The results follow the trends established in Table 3. The major result is that all of the EVA examples meet the allowable failure allocation requirement, but none of the unprotected PVB examples do. Note also that 1 x 4 ft modules and 4 x 4 ft modules give nearly identical results.

CONCLUDING REMARKS

The central finding of this research, upon which the method of module electrochemical breakdown prediction depends, is that a fixed quantity of charge transfer between anode and cathode is required, per unit length of module periphery, to produce a breakdown path; in the experiment described here, that quantity was determined to be about four coulombs per 10 cm of edge. This is a preliminary value obtained from measuring a small number of samples; refined experiments should provide a more precise value for this important quantity.

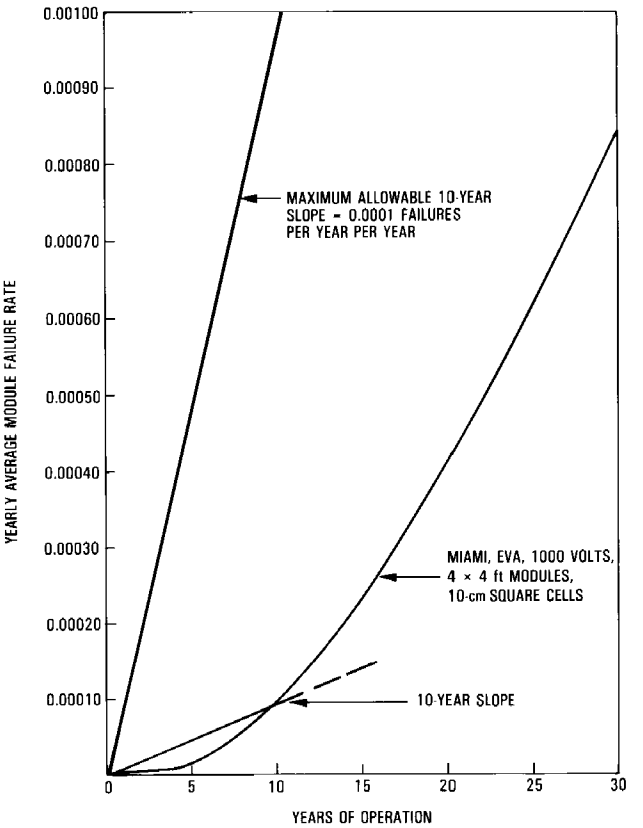

Figure 7. Yearly Average Module Failure Rate versus Years of Operation

The high conductance of PVB is due to its soluble ion content; in a humid environment PVB absorbs a relatively large amount of water (21) and becomes a solid-state electrolyte. Conduction in PVB is essentially ionic in nature. EVA absorbs considerably less water than PVB and is correspondingly less conductive; it is believed that the primary mechanism of conduction in EVA is also ionic (rather than electronic).

In the life-prediction approach presented in this paper, the functional dependence of electrochemical corrosion on encapsulant water content, or its state (22), were not developed; rather, the measured relationship between ambient water content (relative humidity) and polymer conductance was exploited in determining quantity of charge transfer and, hence, median cell life.

In defense of PVB, it should be pointed out that in the experiments reported here, the PVB encapsulant was not protected from the environment, as it would be in actual modules. With proper module design, PVB performs well: if hermetic edge seals and metallized back surface polymer films are used with a glass superstrate, water can be effectively occluded from the PVB encapsulation. Properly designed PVB modules, not necessarily hermetically sealed, have performed acceptably for many years at various applications sites.

Table 4. Slopes of Module Failure-Rate Curves (Failures per Year per Year) for Comparison With Maximum Allowable Slope of 1×10^{-4} Failures per Year per Year

$r = 5$ cm, $\theta_0 = \pi$, $t = 0.114$ cm		Module Failure-Rate Slope							
		Round Cells in PVB				Round Cells in EVA			
		4 x 1 ft		4 x 4 ft		4 x 1 ft		4 x 4 ft	
Cell-to Frame Voltage, V	Cell-to Frame Distance, cm	Boston	Miami	Boston	Miami	Boston	Miami	Boston	Miami
250	0.0635	8.5×10^{-3}	1.0×10^{-1}	1.3×10^{-2}	1.4×10^{-1}	0	2.4×10^{-8}	0	3.8×10^{-8}
	0.635	5.3×10^{-4}	1.0×10^{-2}	8.3×10^{-4}	1.2×10^{-2}	0	0	0	0
1000	0.0635	8.9×10^{-2}	2.8×10^{-1}	1.2×10^{-1}	6.8×10^{-1}	9.5×10^{-8}	8.1×10^{-6}	1.5×10^{-7}	1.3×10^{-5}
	0.635	1.4×10^{-2}	1.0×10^{-1}	8.9×10^{-3}	1.4×10^{-1}	0	1.9×10^{-8}	0	3.1×10^{-8}

$s = 10$ cm, $t = 0.114$ cm		Module Failure-Rate Slope							
		Rectangular Cells in PVB				Rectangular Cells in EVA			
		4 x 1 ft		4 x 4 ft		4 x 1 ft		4 x 4 ft	
Cell-to-Frame Voltage, V	Cell-to-Frame Distance, cm	Boston	Miami	Boston	Miami	Boston	Miami	Boston	Miami
250	0.0635	3.0×10^{-1}	4.4×10^{-3}	4.1×10^{-1}	8.6×10^{-1}	2.5×10^{-6}	9.3×10^{-5}	4.0×10^{-5}	1.5×10^{-4}
	0.635	7.1×10^{-3}	9.3×10^{-2}	1.1×10^{-2}	1.2×10^{-1}	2.1×10^{-10}	3.8×10^{-8}	3.4×10^{-10}	6.0×10^{-8}
1000	0.0635	7.9×10^{-1}	9.5×10^{-1}	8.4×10^{-1}	9.7×10^{-1}	1.6×10^{-4}	2.0×10^{-3}	2.5×10^{-4}	2.8×10^{-3}
	0.635	7.9×10^{-2}	5.5×10^{-1}	1.1×10^{-1}	6.5×10^{-1}	8.6×10^{-8}	6.0×10^{-6}	1.4×10^{-7}	9.6×10^{-6}

On the other hand, EVA-encapsulated modules may require no protection for the EVA since moisture penetration into the EVA is minimal.

ACKNOWLEDGMENTS

The authors acknowledge the efforts of Elizabeth Jetter, Scott Leland, and Timothy Sullivan, without whose skills this work would not have been accomplished.

REFERENCES

1. Ghate, P.B., "Electromigration-induced Failures in VLSI Interconnects," Solid State Technology, pp. 113-120, March 1983.

2. Sbar, N.L., and Feinstein, L.G., "Performance of New Copper Based Metallization Systems in an 85°C 80-percent RH Cl_2 Contaminated Environment," IEEE Transactions on Parts, Hybrids, and Packaging, Vol. PHP-13, No. 3, pp. 208-218, September 1977.

3. Feinstein, L.G., and Sbar, N.L., "Performance of New Copper-based Metallization Systems in an 85°C, 78% RH, SO_2 Contaminated Environment," IEEE Transactions on Components, Hybrids, and Manufacturing Technology, Vol. CHMT-2, No. 2, pp. 159-171, June 1979.

4. Sbar, N.L., and Kozakiewicz, R.P., "New Acceleration Factors for Temperature, Humidity, Bias Testing," IEEE Transactions on Electron Devices, Vol. ED-26, No. 1, pp. 56-71, January 1979.

5. Prince, J., Lathrop, J., Morgan, F., Royal, E., and Witter, G., "Accelerated Stress Testing of Terrestrial Solar Cells," 17th Annual Proceedings, Reliability Physics Symposium, IEEE, pp. 77-86, 1979.

6. Franklin Research Center, A Review of Equipment Aging Theory and Technology, Final Report, September 1980 (prepared for Electric Power Research Institute).

7. Otth, D., and Ross, R., Jr., "Assessing Photovoltaic Module Degradation and Lifetime from Long-Term Environmental Tests," Proceedings--IES, pp. 121-126, 1983.

8. Mon, G., Moore, D., and Ross, R., Jr., "Solar-Cell Interconnect Design for Terrestrial Photovoltaic Modules," ASME Journal of Solar Energy Engineering, 1984.

9. Bacon, C., Smith, J., and Rugg, F., "Electrolytic Resistance in Evaluating Protective Merit of Coatings on Metals," Industrial and Engineering Chemistry, Vol. 40, No. 1, pp. 161-167, 1948.

10. Leidheiser, H., Jr., and Kendig, M., "The Mechanism of Corrosion of Polybutadiene-Coated Steel in Aerated Sodium Chloride," Corrosion-NACE, Vol. 32, No. 2, pp. 69-76, 1976.

11. Leidheiser, H., Jr., "Electrical and Electro-Chemical Measurements as Predictors of Corrosion at the Metal-Organic Coating Interface," Progress in Organic Coatings, Vol. 7, pp. 70-104, 1979.

12. Leidheiser, H., Jr., "Towards a Better Understanding of Corrosion Beneath Organic Coatings," Corrosion-NACE, Vol. 39, No. 5, pp. 189-201, 1983.

13. Davidon, W.C., "Variable Metric Method for Minimization," AEC R & D Report ANL-5990, 1959.

14. Fletcher, R., and Powell, M.J., "Rapidly Convergent Descent Method for Minimization," Computer Journal, Vol. 7, pp. 149-154, 1964.

15. Kallis, J.M., Trucker, D.C., Cuddihy, E., and Garcia, A., "Electrical Isolation Design of Photovoltaic Modules," 17th IEEE Photovoltaic Specialists Conference, Orlando, FL, May 1-4, 1984.

16. Bockris, J.O'M., and Reddy, A.K.N., Modern Electrochemistry, Vols. 1 and 2, Plenum Press, 1970.

17. Ross, R., Jr., "Photovoltaic Design Optimization for Terrestrial Applications," Proceedings of the 13th IEEE Photovoltaic Specialists Conference, pp. 1067-1073, 1978.

18. Ross, R., Jr., "Flat-Plate Photovoltaic Array Design Optimization," Proceedings of the 14th IEEE Photovoltaic Specialists Conference, pp. 1126-1132, 1980.

19. Hines, W., and Montgomery, D., Probability and Statistics in Engineering and Management Science, 2nd Edition, John Wiley & Sons, 1980.

20. Ross, R., Jr., "Technology Developments Toward Thirty-Year-Life Photovoltaic Modules," presented at the 17th IEEE Photovoltaic Specialists Conference, Orlando, FL, May 1-4, 1984.

21. Milby, R.V., "Water Absorption of Polymers," Plastics Technology, McGraw-Hill, 1973.

22. Johnson, G., Bair, M., Matsuoka, S., Anderson, E., Scott, J., "Water Sorption and its Effect on a Polymer's Dielectric Behavior," Water in Polymers, American Chemical Society Symposium Series 127, pp. 451-468, 1980.